

# Geophysical Research Letters<sup>®</sup>



## RESEARCH LETTER

10.1029/2023GL104664

### Key Points:

- Nyiragongo volcano (D.R. Congo) is a permanent emitter of infrasound that pauses during rare flank eruptions
- Intra-crater lava eruptions (lava lake, spatter cone, lava pond) are detected up to the observatory in a dense urban area ~17 km away
- Joint analysis with space-based observations over the period 2018–2022 provides a clear picture of the persistent unrest at this volcano

### Supporting Information:

Supporting Information may be found in the online version of this article.

### Correspondence to:









J. Barrière,  
[julien.barriere@ecgs.lu](mailto:julien.barriere@ecgs.lu)

### Citation:

Barrière, J., Oth, A., d'Oreye, N., Subira, J., Smittarello, D., Brenot, H., et al. (2023). Local infrasound monitoring of lava eruptions at Nyiragongo volcano (D.R. Congo) using urban and near-source stations. *Geophysical Research Letters*, 50, e2023GL104664. <https://doi.org/10.1029/2023GL104664>

Received 23 MAY 2023  
Accepted 5 SEP 2023

## Local Infrasound Monitoring of Lava Eruptions at Nyiragongo Volcano (D.R. Congo) Using Urban and Near-Source Stations

Julien Barrière<sup>1</sup> , Adrien Oth<sup>1</sup> , Nicolas d'Oreye<sup>1,2</sup> , Josué Subira<sup>3,4,5</sup> , Delphine Smittarello<sup>1</sup> , Hugues Brenot<sup>6</sup> , Nicolas Theys<sup>6</sup> , and Benoît Smets<sup>3,7</sup> 

<sup>1</sup>European Center for Geodynamics and Seismology, Walferdange, Luxembourg, <sup>2</sup>Department of Geophysics/Astrophysics, National Museum of Natural History, Luxembourg City, Luxembourg, <sup>3</sup>Natural Hazards and Cartography Service, Royal Museum for Central Africa, Tervuren, Belgium, <sup>4</sup>Goma Volcano Observatory, Goma, D.R. Congo, <sup>5</sup>Department of Geography, Université de Liège, Liège, Belgium, <sup>6</sup>Royal Belgian Institute for Space Aeronomy, Uccle, Belgium, <sup>7</sup>Cartography and GIS Research Group, Department of Geography, Vrije Universiteit Brussel, Brussels, Belgium

**Abstract** During eruptions, volcanoes produce air-pressure waves inaudible for the human ear called infrasound, which are very helpful for detecting early signs of magma at the surface. Compared to violent ash-rich explosions, recording more discrete atmospheric disturbances from effusive eruptions remains a practical challenge depending on the distance to the source. At Nyiragongo volcano (D.R. Congo), towering above a 1-million urban area, we analyzed local infrasonic records between January 2018 and April 2022. An acoustic signature from this open-vent volcano is detected up to the volcano observatory facilities in Goma city center about 17 km from its crater. We compared infrasound signals with space-based observations of the intra-crater activity (SO<sub>2</sub> emissions, thermal anomalies, crater depth/radius). We thus obtain a comprehensive picture of Nyiragongo's eruptive activity during this period, encompassing the drainage of its lava lake during its third known flank eruption on 22 May 2021.

**Plain Language Summary** Similar to seismic waves propagating within the solid Earth, acoustic waves propagate in the atmosphere as a result of near-surface volcanic activity. In contrast with powerful volcanic explosions, close-range deployment of instruments around the active vent (for instance <15 km) is generally needed for continuously monitoring long-living lava effusion or degassing as observed at open-vent volcanoes, such as Kīlauea (Hawaii) or Nyiragongo (D.R. Congo). Nyiragongo hosted the world's largest lava lake up to 2021, which was drained during the third known flank eruption of this volcano on 22 May 2021. While watching for possible reawakening, we detected the infrasound signature of a nascent lava lake four months later, highlighting the crucial role of infrasound monitoring. Remote observations from space (ground deformation, gas emissions, thermal anomalies) can also provide essential information about the eruptive state of a volcano and were jointly analyzed with infrasound records. Knowing that Nyiragongo towers above the 1-million inhabitant city of Goma, such an approach has significant implications for optimizing future monitoring efforts in a harsh field environment.

## 1. Introduction

Exploring the infrasound band (below 20 Hz, inaudible for human ears) with dedicated microphones has become increasingly popular for studying various volcanic eruptive styles from short to long distances (a few to thousands of km) (Fee & Matoza, 2013). For the specific case of open-vent volcanoes where the magmatic pressure within the plumbing system can be released (in contrast with closed edifices), infrasound appears particularly suitable for the continuous recording and characterization of lava lakes (Barrière et al., 2018; Fee et al., 2010; Johnson et al., 2018; Patrick et al., 2016; Valade et al., 2018), degassing vents, inner crater and cavities (Fee et al., 2010; Matoza et al., 2010; Ripepe et al., 2010) or lava fountaining and lava flows (Lyons et al., 2021; Thelen et al., 2022; Olivieri et al., 2013). Strombolian explosions can be effectively recorded from tens of kilometers (Dabrowa et al., 2014) to distances exceeding several hundreds of km (Marchetti et al., 2019). The range-dependent capability of infrasound installations for monitoring long-lived Hawaiian style lava effusion is generally constrained to local distances (<15 km), as evidenced at Kīlauea, Hawaii (Fee & Garcés, 2007; Garcés et al., 2003; Thelen et al., 2022). Depending on the source energy, such a local monitoring can be hampered by atmospheric effects, where wind is the main source of infrasound noise that can mask volcanic signals (Fee & Garcés, 2007). Path effects due to the topography can be significant at local scale, altering the waveform (Lacanna & Ripepe, 2013)

© 2023 The Authors.

This is an open access article under the terms of the [Creative Commons Attribution-NonCommercial License](https://creativecommons.org/licenses/by-nc/4.0/), which permits use, distribution and reproduction in any medium, provided the original work is properly cited and is not used for commercial purposes.

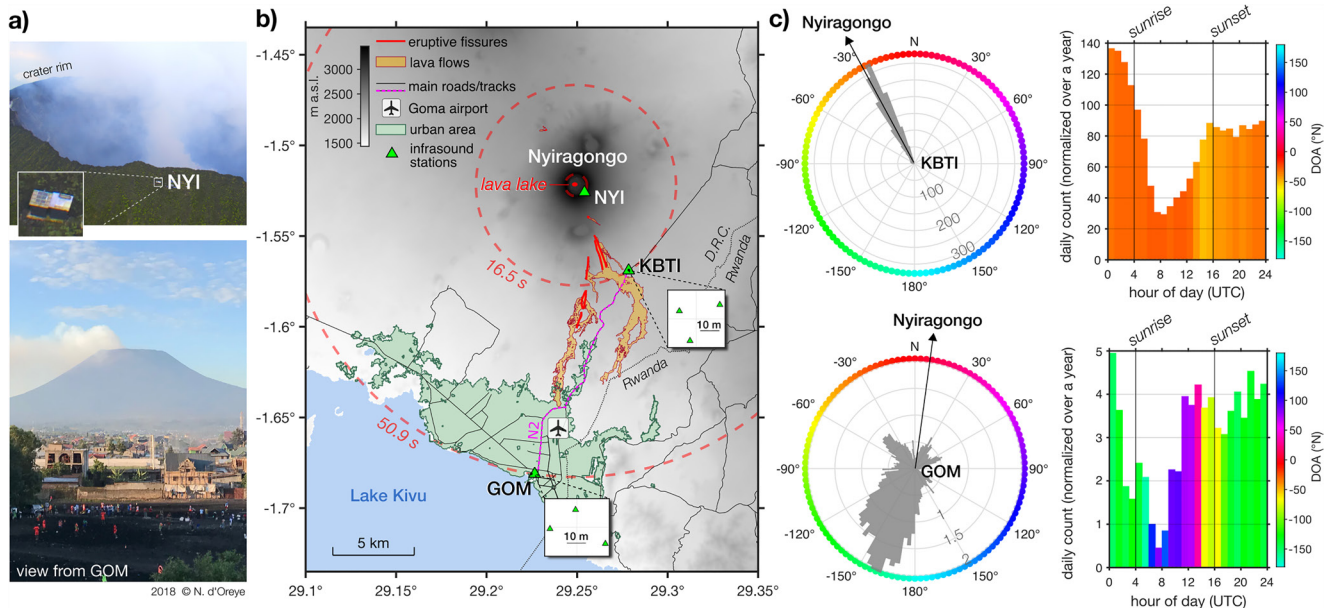


**Figure 1.** (a) Nyiragongo as viewed from the Goma Volcano Observatory (station GOM) and at the summit (station NYI) in 2018. (b) Map of the study area depicting the limits of the urban area (Michellier et al., 2016), the eruptive fissures and the lava flows of the 2021 flank eruption (Smittarello et al., 2022). The locations of the infrasound stations are represented by green triangles with two insets for KBTI and GOM showing the configuration of the three-element arrays. Circular red dashed lines correspond to the 2-D propagation of an infrasound wavefront from Nyiragongo's crater. The main roads are plotted from data sets available at the WFP geonode. The boundary R.D.C/Rwanda is plotted accordingly to the 2015 GADM database. The background topography is derived from SRTM data with 1 arc-second resolution (NASA/United States Geological Survey). (c) Daily count of infrasound detections at KBTI and GOM between 22 May 2020 and 22 May 2021 00:00 UTC, represented as a function of direction of arrival (DOA) (left polar plots) and hour of day (UTC time) (right histograms). An event is declared when the normalized cross-correlation coefficient between signals of the 3-element array exceeds a threshold of 0.6. Counts over the 1-year period are normalized by the number of days with available data, giving average daily counts. The average DOA per hour of day (color scale in histograms) are obtained by calculating the circular mean (Berens, 2009).

and resulting in biased source locations if straight-line propagation is assumed (Fee et al., 2021). In case of a dense urban area nearby, human activity can also be an issue, since the anthropogenic acoustic noise at infrasound frequencies can reduce the detectability of other signals (McComas et al., 2022). Finally, microbaroms generated over the oceans are a dominant source of ambient noise recorded worldwide around 0.1–0.4 Hz (Bowman et al., 2005) and can contaminate volcanic signals (Fee et al., 2010; Rosenblatt et al., 2022).

Nyiragongo, located in the Virunga Volcanic Province, is one of the most active volcanoes on Earth (Wright et al., 2015) (Figure 1a). Together with its neighbor Nyamulagira located around 14 km away, Nyiragongo is an important emitter of sulfur dioxide ( $\text{SO}_2$ ) characterized by continuous passive degassing (Carn et al., 2016). The effusive activity within its ~1.2 km wide crater takes the form of a lava lake most of the time (Barrière et al., 2022). On 22 May 2021, the lava lake was drained and the inferred shallow dyke intrusion propagated up to Lake Kivu without any obvious precursory signs (seismicity, deformation, gas emissions, infrasound) as documented by Smittarello et al. (2022). For the third time in Nyiragongo's known eruptive history after January 1977 and 2002, lava escaped from fissures opening along Nyiragongo's southern flank, rapidly reaching the northern limits of the urban area and ultimately entering the city of Goma, which nowadays hosts about 1 million inhabitants (Syavulisembo et al., 2021) (Figures 1a and 1b). A few months later, the intermittent reappearance of lava within Nyiragongo's central crater was confirmed by the Goma Volcano Observatory (GVO) between September and November 2021 (Global Volcanism Program, 2021).

Between 2013 and 2016, two infrasound arrays were deployed in safe places in the framework of the seismic network KivuSNet (Oth et al., 2017): the Virunga Park rangers' building (station KBTI, ~5.6 km away from the crater rim) and the GVO's facilities in the city center of Goma (station GOM, ~17.3 km away). An additional stand-alone sensor on Nyiragongo's rim (station NYI) was deployed at the summit in early 2018 and fully operational by the end of 2019 (Figures 1a and 1b). Near-source infrasound stations (i.e., flank and summit) already provided insights into the eruptive dynamics of Nyiragongo (Barrière et al., 2018; Valade et al., 2018). However, operating an infrasound station like GOM in a dense urban area is challenging (McComas et al., 2022) and has

not been adequately tested or explored worldwide. If an infrasound station deployed in a city detects a coherent and meaningful signal, it could reduce the need for a dangerous geophysical deployment, overcoming possible accessibility, security and/or budgetary issues.

Alongside the use of infrasound sensors, space-based observations are also an efficient complement for monitoring eruptive activity. The analysis of radar amplitude images acquired by Synthetic-Aperture Radar (SAR) satellite sensors offers the opportunity to detect morphology changes of volcanic craters as evidenced at African lava-lake volcanoes Nyiragongo, D.R. Congo (Barrière et al., 2018, 2022; Smittarello et al., 2023), its neighbor Nyamulagira (Burgi et al., 2021) and Erta' Ale, Ethiopia (Moore et al., 2019). Sulfur dioxide is a key constituent of volcanic plumes which can be measured from space-based spectrometers owing to its distinct absorption spectral signature in the ultraviolet (e.g., Carn et al., 2016; Theys et al., 2019). Space-based instruments with infrared capabilities allow for the detection of thermal anomalies (hotspots) related to volcanic activity (e.g., Marchese et al., 2019; Massimetti et al., 2020). These multidisciplinary data (i.e., crater geometry, SO<sub>2</sub> emissions, hotspots) will be jointly analyzed in this study with infrasound records.

## 2. Infrasound Data Processing

### 2.1. Single-Station Array Processing

KBTI and GOM stations are both equipped with three sensors, which are portable and cost-effective infraBSU instruments (corner frequency of 10 s) manufactured by Boise State University (Johnson et al., 2012). They are connected to the same acquisition system with a small aperture of ~20-m between sensors, similar to other local deployments at volcanoes (Johnson & Ronan, 2015; Yamakawa et al., 2018). Deploying at least three sensors at the same site allows performing array processing for retrieving the direction of arrival (DOA) and an apparent velocity ( $V_{app}$ ) of coherent waves passing through the array. Based on their array responses (Figures S1 and S2 in Supporting Information S1), these two deployments are efficient at detecting coherent infrasound arrivals in the frequency range 1–8 Hz. Standard least squares beamforming (De Angelis et al., 2020) is applied to each 3-element array for successive windows of 10-s length overlapped by 50%.

### 2.2. Multi-Station Processing

If a signal coming from Nyiragongo is recorded at different stations, the spacing between sensors by a minimum of 5.5 km (inter-station distance NYI-KBTI) allows exploring a wider frequency band than the single-station approach down to 0.1 Hz (i.e., at least 1.5 infrasonic wavelengths between NYI and KBTI). Assuming sub-horizontal plane wave propagation with apparent velocity close to the adiabatic sound speed ( $V_{app} \sim 340$  m/s), red dashed lines in Figure 1b mimic the atmospheric propagation of a circular wavefront of a signal originating from Nyiragongo's crater. Such a signal would take ~50 s to reach GOM in GVO's facilities on the shore of Lake Kivu.

Cross-correlating continuous infrasound signals acquired at both locations can be useful for identifying coherent signals across a station pair, as commonly done in ambient seismic noise processing (Bensen et al., 2007). As sole pre-processing procedures, data are filtered between 0.1 and 10 Hz and normalized in time domain using the running-absolute-mean method in order to enhance continuous signals (Bensen et al., 2007). The final cross-correlation functions (CCFs) are calculated from successive 10-min signal segments with 50% overlap, thus leading to 5-min time sampling.

Picking the maximum coefficient of each CCF allows determining the time lag needed for the dominant infrasound signal to reach one station after the other. Cross-correlating 10 min-long segments with minimal pre-processing will generally result in very low cross-correlation coefficients. A straightforward solution for differentiating periods with clear and no clear infrasound wave arrival is to compute the signal-to-noise ratio (SNR) of the CCFs. We choose the following definition (Yang & Ritzwoller, 2008):  $SNR = \text{max}/\text{noise}$ , where max is the peak amplitude of the CCFs in a time lag window corresponding to a potential wave arrival originating from Nyiragongo and noise is the rms (root-mean-square) amplitude of the CCFs outside the signal window.

## 3. Space-Based Complementary Observations

### 3.1. Lava-Lake Pit Crater Depth and Radius

Barrière et al. (2022) set up an automatic method called SAsHa (SAR shadows analysis) based on the simple principle that SAR signals (radar beam along a line of sight) impinging on a natural or man-made structure cast

shadow proportional to its height. At Nyiragongo, time series of the lava-lake level, elevation and mean radius of the pit crater rim were obtained from a dense data set of satellite images over about 20 years (2002–2021). Smittarello et al. (2023) developed the method called PickCraterSAR, which extend the applicability of SAR amplitude when the layover effect limits the maximum depth reachable by the SAsa method (see both studies for more details). In the present study, we provide the merged data set between SAsa and PickCraterSAR up to July 2021 and extend the time series with newly processed COSMOSkyMed images up to April 2022.

### 3.2. SO<sub>2</sub> Emissions

The TROPOMI instrument on board the Sentinel-5P satellite samples the Earth's atmosphere once a day with unprecedented spatial resolution of  $3.5 \times 5.5$  km<sup>2</sup>, which allows differentiating SO<sub>2</sub> emissions from very close volcanoes such as Nyiragongo and Nyamulagira (Theys et al., 2019). TROPOMI SO<sub>2</sub> vertical column data from the S5P operational processing algorithm (Theys et al., 2017) are used to estimate daily SO<sub>2</sub> mass, by summing up the data over the entire detected SO<sub>2</sub> plume. For this, we assume the volcanic plume from Nyiragongo to be about 1 km above its summit, in a 1-km thick layer (Theys et al., 2019).

### 3.3. Thermal Anomalies

The multi-spectral instruments on-board Sentinel-2 and Landsat-8 satellites allow a spatial resolution of 20 and 30 m in the Short Wave Infrared bands, respectively (Marchese et al., 2019). We applied the HOTMAP algorithm (Murphy et al., 2016) for highlighting the thermal radiation of Nyiragongo's intra-crater lava eruptions (lava lake, spatter cone, lava flows, hot gas plume). Sentinel-2 and Landsat-8 results (complemented by Landsat-9 data since 5 November 2021) are merged by multiplying hotspot pixel counts by the area of the pixel (in m<sup>2</sup>). Note that both underestimation and overestimation of hot pixels can often occur due to the presence of volcanic and/or water clouds (e.g., Massimetti et al., 2020).

## 4. Infrasound Monitoring Results

### 4.1. Single-Station Approach

Figure 1c depicts daily statistics of infrasound events (counts per Direction of Arrival—DOA—and hour of day) at KBTI and GOM arrays over a year-long period (May 2020–2021) when a persistent active lava lake was observed prior to the May 2021 eruption (Barrière et al., 2022) (See also Figures S3 and S4 in Supporting Information S1). The number of detections at KBTI is more than 25 times higher than at GOM. A vast majority of infrasound signals retrieved at KBTI are coming from Nyiragongo while most of the detections at GOM indicate infrasound sources to the southwest. There is a clear diurnal effect within the shallow Atmospheric Boundary Layer affecting wave propagation path and amplitude due to changing temperature and wind conditions (e.g., Fee & Garcés, 2007; Marcillo et al., 2015; Smink et al., 2019). At both locations, the number of detections is significantly reduced during daytime. At GOM, this also leads to reversed DOA to the east-northeast. Nearby anthropogenic activities (e.g., airport, military operations, construction) are potential additional sources of noise (McComas et al., 2022). Detections at GOM during working hours could thus include both anthropogenic and natural events from distant and local sources. However, there is no evidence of daily repetitive events originating from the volcano. On the contrary, the DOA remains quite stable at KBTI, pointing throughout the day at Nyiragongo.

### 4.2. Multi-Station Approach

CCFs of successive 10-min segments are computed for three station pairs (only one sensor is chosen for KBTI and GOM). The result is displayed as a map of daily CCFs envelopes (2D plane “time lag vs. date”) obtained by averaging 10-min CCFs over 1-day lagging window (Figure 2a). Clear single maxima (red color range) are observed at positive and nearly constant time lags  $t_{\text{obs}}$  of 16.5, 34, and 50.5 s (with standard deviations of  $\sim 0.08$ , 0.13, and 0.17 s, respectively) as the inter-stations' distance increases (5.6, 11.7, and 17.3 km, respectively). Assuming a straight-line propagation and a wave speed of 340 m/s, the theoretical differential travel times  $t_{\text{theo}}$  from a signal generated at Nyiragongo's lava lake is respectively 16.5, 34.4, and 50.9 s for the corresponding inter-station distances (Figure 1b). Considering the above-mentioned simplified assumptions, observed and

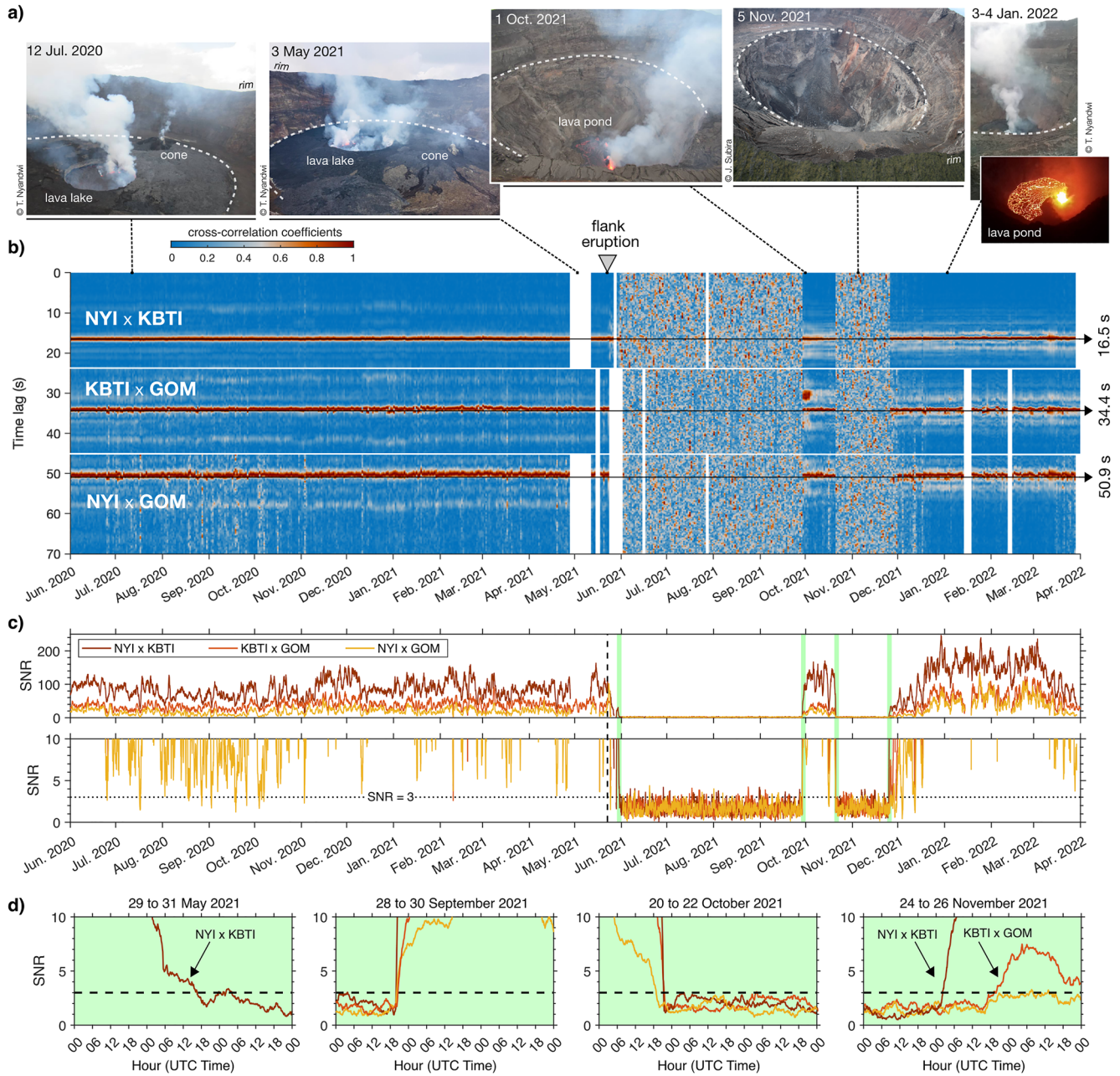


**Figure 2.** (a) Pictures of Nyiragongo's crater (courtesy of T. Nyandwi except the picture taken from a helicopter flight on 5 November 2021 by J. Subira). (b) Normalized Hilbert envelopes of cross-correlation functions (CCFs) displayed in a plane “date versus time lag.” Daily windows with less than 10% of calculated CCFs are ignored (blank parts). Only sections around the single maxima for each station pair are plotted (see Figure S6 in Supporting Information S1). All single CCFs are scaled by their maximum (in red). Theoretical travel-times from a source at Nyiragongo are indicated by horizontal black lines. (c) Signal-to-noise ratio from averaged CCFs calculated over 1-day lagging windows using a 5-min sampling interval. A zoom for values between 0 and 10 is plotted below. (d) Zoom into 3-day period highlighted in panel (c).

theoretical values fit remarkably well and prove that infrasonic waveforms are only marginally distorted between the crater rim and the GVO. The CCFs were filtered in the band [0.4–2] Hz, which is found to be optimal over the entire time period for retrieving coherent signals from Nyiragongo (See Section 6 and Figures S5 and S6 in Supporting Information S1).

The SNR plotted in Figure 2c are extracted from averaged 10-min CCFs over 1-day lagging window with 5-min sampling interval. Using a 1-day lagging window smooths diurnal effects and preserves the temporal onset of

variations. Lower SNR are observed with increasing inter-station distance and distance to Nyiragongo's source due to path effects (i.e., the best pair is NYI  $\times$  KBTI and the worst is NYI  $\times$  GOM). Visual observations taken at the summit (Figure 2a) strongly suggest that the overall loss of correlation for several months in 2021 (June to September, November) is related to the absence of lava eruptions. Zooming into these specific transition periods (Figure 2d) shows that each fading or onset of correlation is well detected with high temporal resolution for the three station pairs (GOM was unfortunately not operational during several days right after the flank eruption). It is worth noting that the last increase of SNR in November 2021 is more progressive than in September and became noticeable for the station pair NYI  $\times$  KBTI about 18 hr before the pair KBTI  $\times$  GOM. The pair NYI  $\times$  GOM does not yet allow to pinpoint the signature of Nyiragongo's source during the same period (after assuming the threshold  $\text{SNR} \geq 3$ ). This implies that the source amplitude during the first hours of this new eruptive event is evidently too low to be detected at GOM and that a too large inter-station distance may additionally hamper the detection of coherent arrivals.

## 5. Nyiragongo's Eruptive Activity in the Period 2018–2022

From a monitoring perspective, we may define a flag indicator of Nyiragongo's infrasound source by merging the time delays and SNR detection criteria defined previously. In Figure 3, we plot a binary indicator where 1 (“yes”) indicates if, for any station pairs,  $t_{\text{obs}}$  falls within the interval  $t_{\text{theo}} \pm 1$  s and  $\text{SNR} \geq 3$ , and 0 (“no”) indicates otherwise. Before 2020, this parameter is almost entirely derived from the pair KBTI  $\times$  GOM. Still in Figure 3a, we plot the infrasound amplitude (one rms value for 10-min window) at KBTI, which has the best data completeness. It is affected by large diurnal variations so the daily median (in red) is plotted onto this 10-min curve (gray). Complementary information on the crater's morphology changes (Sasha and PickCraterSAR methods),  $\text{SO}_2$  emission (TROPOMI/Sentinel-5P) and thermal hotspots (Sentinel-2 and Landsat-8/9) are added for providing an overview of Nyiragongo's eruptive activity from January 2018 (start of TROPOMI observations) to April 2022 (end of operation for the KivuSNet infrasound stations).

According to the infrasound flag indicator, Nyiragongo's lava lake was a persistent emitter of infrasound detected at GVO before the 2021 flank eruption. High  $\text{SO}_2$  emissions are synchronous with drops of the lava-lake level as clearly observed for the three successive degassing peaks in April–August 2019 (Theys et al., 2021). These amplitude peaks are also detected in the infrasound records at KBTI. Between late 2019 and early 2020, all parameters conveyed the highest unrest for the entire period 2018–2022 more than a year before the flank eruption. Peaks and sustained high levels of infrasound amplitude (night and day),  $\text{SO}_2$  emissions, thermal hotspots and lava-lake surface (including spatter cone activity) lasted several months. These signals ended with a major lava-lake level drop in April 2020, which was associated, according to seismicity, to a deep magmatic intrusion beneath the edifice toward the northeast (Barrière et al., 2022). This kind of dyking events with surface manifestations occurred several times in the past two decades and at least four times in the period studied here: February 2018, October 2018, from April to August 2019 and in April 2020.

The lowest levels of infrasound amplitude at KBTI and loss of correlation between stations (flag = 0) were obtained when the crater was deep and empty after the May 2021 flank eruption, as confirmed by rare pictures taken at the summit (Figure 2a) and satellite images (Figure S7 in Supporting Information S1). Peaks in infrasound amplitude and  $\text{SO}_2$  emissions occurred during the eruption on 22 May while the lava lake was draining (Smittarello et al., 2022). Nyiragongo's infrasound source remained active more than a week after the eruption until 31 May 2021 (Figure 2d). The absence of observable lava-related thermal anomaly was noticed one day later on 1 June 2021 (Figure S7 in Supporting Information S1). This date corresponds to the deepest crater bottom after successive deepening and enlarging of the pit crater ( $\sim 580$  m deeper than before the eruption), after which the crater refilled the crater bottom from collapsing walls (Smittarello et al., 2023). Both renewal of intra-crater activity on 28 September and 25 November 2021 are clearly identified in the infrasound records, further validated by thermal imagery on 29 September despite very cloudy conditions (Figure S8 in Supporting Information S1) or by visual inspection on 1 October (Figure 2a). On 25 November 2021, the acoustic signature from the crater likely revealed the renewal of lava eruption, as confirmed on 27 November by visual observations from GVO at the summit (Global Volcanism Program, 2021). Since this date, the continuous eruption recorded by the infrasound sensors ultimately formed a nascent lava lake within Nyiragongo's crater, similar to those observed between the historical flank eruptions (1977, 2002, and 2021), which could remain highly active or become encrusted over time (Barrière et al., 2022).  $\text{SO}_2$  emissions and thermal hotspots did not show such a clear and/or synchronous

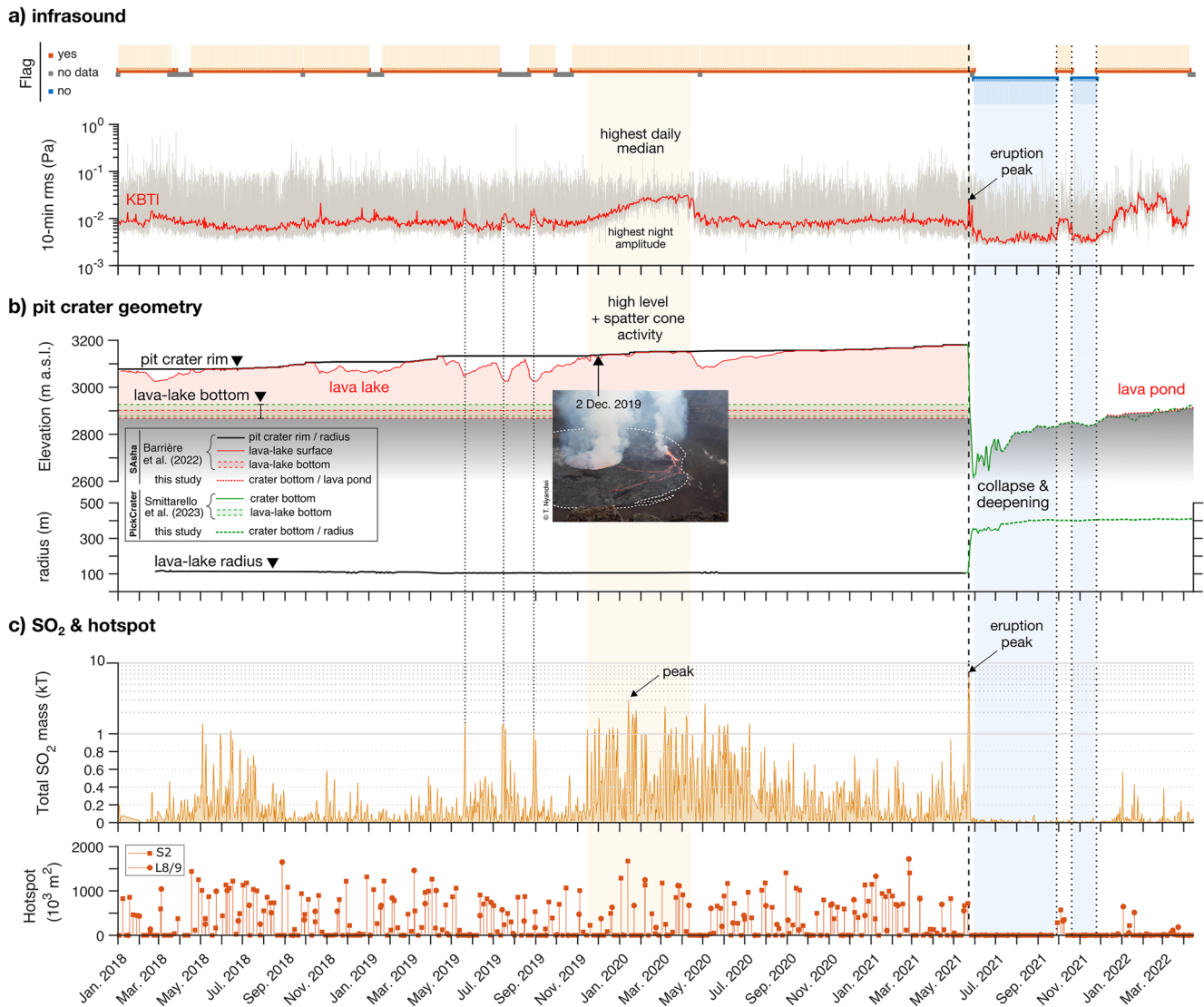


**Figure 3.** (a) Flag indicator for Nyiragongo's source (see the main text). Below, 10-min RMS amplitude at KBTI (gray) and moving daily median (red). Results are obtained in the band [0.4–2] Hz. (b) Pit crater geometry (elevation and radius) using PickCraterSAR and SAsha methods, including the variations of the lava-lake level (in red). Estimates of the lava-lake bottom before the flank eruption are obtained from space-based photogrammetry and SAR images in 2002–2003 when the crater was empty (see Barrière et al. (2022) and Smittarello et al. (2023) for more details). PickCraterSAR data are smoothed with a  $\pm 1$  day moving average window (Smittarello et al., 2023) or  $\pm 7$  days for updated results based on COSMOSkyMed images only. (c) Space-based daily solutions for SO<sub>2</sub> emissions obtained from TROPOMI and thermal hotspots associated to Nyiragongo (S2 stands for Sentinel-2, L8/9 for Landsat-8/9).

increase. Since early 2022, all parameters are indicative of the renewal of sustained activity. The presence of an active lava lake was still noticed one year later by GVO in February 2023 (Global Volcanism Program, 2023).

## 6. Characteristics of Nyiragongo's Infrasound Signature

A few studies performed in recent years provide insights into the source mechanisms of the persistent Nyiragongo's infrasound signature before the May 2021 eruption. Using close-range sensors deployed during a 2-day experiment in April 2016, Valade et al. (2018) explored the acoustic wavefield within the crater in the frequency band 0.5–10 Hz. They characterized the main infrasonic sources as the persistent spattering at the lava lake's surface and the intermittent spatter cone activity alternating between quiescent, effusive and more vigorous explosive phases. Using colocated seismo-acoustic records at KBTI over  $\sim 2$  years (September 2015–November 2017), Barrière et al. (2018) identified long-period ( $< 2$  Hz) repetitive seismic events and continuous tremor (i.e.,

a persistent pressure perturbation) associated with infrasonic emissions and originating from Nyiragongo's crater. Similar to Richardson et al. (2014) at Villarica volcano, Barrière et al. (2018) interpreted these seismo-acoustic signals as related to the large and persistent bubble bursting at the lava lake's surface. Barrière et al. (2019) confirmed the shallow mechanism of the lava-lake generated tremor by comparing intra-crater seismic records with stereographic time-lapse camera in September 2011 (i.e., before the appearance of the spatter cone in March 2016). As observed at Halema'uma'u lava lake (Patrick et al., 2016), the amplitude of the continuous lava-lake tremor is modulated by the alternance of spattering and gas pistonning phases.

Inter-station correlation (CCFs) emerging to a lesser extent in the low (0.1–0.4) and high frequency bands (2–10 Hz) also highlight the broadband nature of the infrasound tremor generated at Nyiragongo (Figures S5 and S6 in Supporting Information S1). Discernible at night, its amplitude is of the order of  $10^{-1}$  Pa at the summit (NYI),  $10^{-2}$  Pa at GOM and in-between at KBTI. The amplitude range recorded at NYI and KBTI is lower by one to two orders of magnitude than recurrent explosion signals or tremors observed at other open-vent volcanoes at similar local distance, for example, at Villarica, Chile (Johnson et al., 2018; Ripepe et al., 2010), or Etna, Italy (De Angelis et al., 2020; Olivieri et al., 2013). A background tremor amplitude around  $10^{-1}$  Pa is closer to levels retrieved at Kīlauea for a distance of less than 7 km from Halema'uma'u lava lake (Patrick et al., 2016). Note that the station NYI was deployed behind the crater rim for technical reasons (see Figure 1a) and the measured infrasound pressure level is most likely affected by the steep near-source topography (Lacanna & Ripepe, 2013).

CCFs in the low (0.1–0.4) and high frequency bands (2–10 Hz) depict higher SNR values after the flank eruption when an active source from the crater is identified (Figure S6 in Supporting Information S1), which convey stronger infrasound emissions (as also observed in the 10-min rms amplitude timeseries at KBTI, Figure 3a). Contrary to the pre-eruptive state characterized by persistent tremor signals, other tremor patterns are significant, like the transition to periodic appearance of hour-long signals to continuous tremor during the renewal of activity in December 2021 (Figures S9 and S10 in Supporting Information S1). Because a large lava lake and a spatter cone disappeared, the changing source properties (Rosenblatt et al., 2022) and modified acoustic response of the crater due to evolving geometry (Watson et al., 2019) can largely influence the frequency and amplitude content of this new infrasound signature. During the May 2021 eruption lasting only ~6 hr (Smittarello et al., 2023), the draining of the lava lake and the lava fountaining on the flank can also be tracked using records from KBTI and NYI (Barrière et al., 2023). These aspects, which are beyond the scope of this paper, will be tackled in a dedicated study. Nevertheless, it is noteworthy that the frequency range [0.4–2] Hz remains the best band for monitoring Nyiragongo's intra-crater infrasound signature after the 2021 eruption.

## 7. Conclusions

At Nyiragongo, deploying only a few infrasound sensors is highly relevant for detecting major variations of intra-crater effusive activity. Space-based products (crater's morphology, SO<sub>2</sub> emissions, thermal hotspots) and occasional visual inspections at the summit complement well the (near) real-time assessment of the eruptive unrest derived from infrasound records. The recurrent political instability and civil wars in the whole Kivu region remain however an important concern for the long-term sustainability of such ground-based monitoring infrastructures. At the time of writing (early 2023), the civil war zone has extended to the southern territory of Nyiragongo, limiting the access to NYI and KBTI stations (GVO Pers. Comm.). The harsh field environment near Nyiragongo leads to the need for an easily accessible and protected location for instrument deployment, which, in the context of Goma, likely resides within the confines of the city. The sole deployment of another “city-based” infrasound microphone at a different secure location from GVO (ideally closer to Nyiragongo) may also be a good strategy to extract meaningful information through a unique pair of urban stations. The presence of a growing lava lake with major level drops associated with deep dyke intrusions has been a permanent marker of sustained pressure build-up for the past two decades (Barrière et al., 2022), accelerating since mid-2015 (Walwer et al., 2023) up to the sudden occurrence of the May 2021 flank eruption triggered by edifice rupture (Smittarello et al., 2022). The fast return of fresh lava within its crater reflects once more the persistent unrest at Nyiragongo and the need to monitor its acoustic signature consistently.

## Data Availability Statement

Sentinel-2 and TROPOMI data are available from the ESA Copernicus Open Access, that is, for Sentinel-2: <https://scihub.copernicus.eu/dhus/#/home> (satellite platforms “S2A\_\*” and “S2B\_\*” and product “S2MSI1C” in the search bar) and for TROPOMI: <https://s5phub.copernicus.eu/dhus/#/home> (Product “L2\_SO2\_” in the search bar). Landsat-8/9 data are provided by the USGS and can be downloaded from the Google Earth Engine



platform, that is, for Landsat-8: [https://developers.google.com/earth-engine/datasets/catalog/LANDSAT\\_LC08\\_C02\\_T1\\_RT\\_TOA](https://developers.google.com/earth-engine/datasets/catalog/LANDSAT_LC08_C02_T1_RT_TOA), and for Landsat-9: [https://developers.google.com/earth-engine/datasets/catalog/LANDSAT\\_LC09\\_C02\\_T1\\_TOA](https://developers.google.com/earth-engine/datasets/catalog/LANDSAT_LC09_C02_T1_TOA). COSMOSkyMed data (ISA) are available from the Virunga Supersite Initiative (<https://geo-gsnl.org/supersites/permanent-supersites/virunga-supersite/>). Infrasound data archiving and accessibility from KivuSnet is ensured through the GEOFON program of the GFZ German Research Centre for Geosciences (<https://doi.org/10.14470/XI058335>) under the KV FDSN code (<http://www.fdsn.org/networks/detail/KV/>).

#### Acknowledgments

We would like to thank the people at GVO involved in the operation of KivuSnet (infrasound stations) and the sentinels of the monitoring stations. We thank T. Nyandwi for providing us his photos of Nyiragongo's crater and the Virunga National Park for hosting the stations KBTI and NYI. We thank the MONUSCO (UN stabilization mission in Congo) for organizing helicopter flights to Nyiragongo's crater for GVO. We are grateful to the European Space Agency (ESA) and the United States Geological Survey (USGS) for providing the Sentinel-2 and Landsat-8/9 products for free, respectively, to Belgian Science Policy Office (BELSPO) and the Virunga Supersite Initiative for funding COSMOSkyMed images (ISA - Italian Space Agency). The work related to TROPOMI SO<sub>2</sub> data was performed in the frame of the TROPOMI project. We acknowledge financial support from ESA's Sentinel-5P and Belgium's Prodex TRACE-S5P projects. Thermal and SO<sub>2</sub> data were processed in the frame of the VeRSUS project (BELSPO, STEREO-III Programme, Contract SR/00/382). The array processing of infrasound records has been adapted from the software implementation of least-square beamforming provided by De Angelis et al. (2020), available at <https://github.com/silvioda/Infrasound-Array-Processing-Matlab>. The authors would like to thank two anonymous reviewers for their constructive comments that have helped us improve the former manuscript.

#### References

- Barrière, J., d'Oreye, N., Oth, A., Theys, N., Mashagiro, N., Subira, J., et al. (2019). Seismicity and outgassing dynamics of Nyiragongo volcano. *Earth and Planetary Science Letters*, 528, 115821. <https://doi.org/10.1016/j.epsl.2019.115821>
- Barrière, J., Nicolas, D., Smets, B., Oth, A., Delhaye, L., Subira, J., et al. (2022). Intra-Crater eruption dynamics at Nyiragongo (D.R. Congo), 2002–2021. *Journal of Geophysical Research: Solid Earth*, 127(4), 2002–2021. <https://doi.org/10.1029/2021JB023858>
- Barrière, J., Oreye, N., Oth, A., Geirsson, H., Mashagiro, N., Johnson, J. B., et al. (2018). Single-station seismo-acoustic monitoring of Nyiragongo's lava lake activity, D.R. Congo. *Frontiers in Earth Science*, 6. <https://doi.org/10.3389/feart.2018.00082>
- Barrière, J., Oth, A., Subira, J., Smets, B., & D'Oreye, N. (2023). Infrasonic noise from lava eruptions at Nyiragongo volcano, D.R. Congo. In *SSA 2023 annual meeting, seismological Research Letters* (Vol. 94, p. 1157). <https://doi.org/10.1785/0220230054>
- Bensen, G. D., Ritzwoller, M. H., Barmin, M. P., Levshin, A. L., Lin, F., Moschetti, M. P., et al. (2007). Processing seismic ambient noise data to obtain reliable broad-band surface wave dispersion measurements. *Geophysical Journal International*, 169(3), 1239–1260. <https://doi.org/10.1111/j.1365-246X.2007.03374.x>
- Berens, P. (2009). CircStat: A MATLAB toolbox for circular statistics. *Journal of Statistical Software*, 31(10). <https://doi.org/10.18637/jss.v031.i10>
- Bowman, J. R., Baker, G. E., & Bahavar, M. (2005). Ambient infrasound noise. *Geophysical Research Letters*, 32(9), 1–5. <https://doi.org/10.1029/2005GL022486>
- Burgi, P. Y., Valade, S., Coppola, D., Boudoire, G., Mavonga, G., Rufino, F., & Tedesco, D. (2021). Unconventional filling dynamics of a pit crater. *Earth and Planetary Science Letters*, 576, 117230. <https://doi.org/10.1016/j.epsl.2021.117230>
- Carn, S. A., Clarisse, L., & Prata, A. J. (2016). Multi-decadal satellite measurements of global volcanic degassing. *Journal of Volcanology and Geothermal Research*, 311, 99–134. <https://doi.org/10.1016/j.jvolgeores.2016.01.002>
- Dabrowa, A. L., Green, D. N., Johnson, J. B., Phillips, J. C., & Rust, A. C. (2014). Comparing near-regional and local measurements of infrasound from Mount Erebus, Antarctica: Implications for monitoring. *Journal of Volcanology and Geothermal Research*, 288, 46–61. <https://doi.org/10.1016/j.jvolgeores.2014.10.001>
- De Angelis, S., Haney, M. M., Lyons, J. J., Wech, A., Fee, D., Diaz-Moreno, A., & Zuccarello, L. (2020). Uncertainty in detection of volcanic activity using infrasound arrays: Examples from Mt. Etna, Italy. *Frontiers in Earth Science*, 8(May), 1–11. <https://doi.org/10.3389/feart.2020.00169>
- Fee, D., & Garcés, M. (2007). Infrasonic tremor in the diffraction zone. *Geophysical Research Letters*, 34(16), 1–5. <https://doi.org/10.1029/2007GL030616>
- Fee, D., Garcés, M., Patrick, M., Chouet, B., Dawson, P., & Swanson, D. (2010). Infrasonic harmonic tremor and degassing bursts from Halema'uma'u Crater, Kilauea Volcano, Hawaii. *Journal of Geophysical Research*, 115(11), 1–15. <https://doi.org/10.1029/2010JB007642>
- Fee, D., & Matoza, R. S. (2013). An overview of volcano infrasound: From Hawaiian to Plinian, local to global. *Journal of Volcanology and Geothermal Research*, 249, 123–139. <https://doi.org/10.1016/j.jvolgeores.2012.09.002>
- Fee, D., Toney, L., Kim, K., Sanderson, R. W., Iezzi, A. M., Matoza, R. S., et al. (2021). Local explosion detection and infrasound localization by reverse time migration using 3-D finite-difference wave propagation. *Frontiers in Earth Science*, 9(February), 1–14. <https://doi.org/10.3389/feart.2021.620813>
- Garcés, M., Harris, A., Hetzer, C., Johnson, J., Rowland, S., Marchetti, E., & Okubo, P. (2003). Infrasonic tremor observed at Kilauea Volcano, Hawaii. *Geophysical Research Letters*, 30(20), 2023. <https://doi.org/10.1029/2003GL018038>
- Global Volcanism Program. (2021). Report on Nyiragongo (D.R. Congo), bulletin of the global volcanism network (Vol. 46, p. 12).
- Global Volcanism Program. (2023). Report on Nyiragongo (D.R. Congo). In S. K. Sennert (Ed.), *Weekly volcanic activity report, 22 February-28 February 2023*. Smithsonian Institution and US Geological Survey.
- Johnson, J. B., Anderson, J., Marcillo, O., & Arrowsmith, S. (2012). Probing local wind and temperature structure using infrasound from Volcan Villarrica (Chile). *Journal of Geophysical Research*, 117(D17), D17107. <https://doi.org/10.1029/2012JD017694>
- Johnson, J. B., & Ronan, T. J. (2015). Infrasound from volcanic rockfalls. *Journal of Geophysical Research: Solid Earth*, 120(12), 8223–8239. <https://doi.org/10.1002/2015JB012436>
- Johnson, J. B., Watson, L. M., Palma, J. L., Dunham, E. M., & Anderson, J. F. (2018). Forecasting the eruption of an open-vent volcano using resonant infrasound tones. *Geophysical Research Letters*, 45(5), 2213–2220. <https://doi.org/10.1002/2017GL076506>
- Lacanna, G., & Ripepe, M. (2013). Influence of near-source volcano topography on the acoustic wavefield and implication for source modeling. *Journal of Volcanology and Geothermal Research*, 250, 9–18. <https://doi.org/10.1016/j.jvolgeores.2012.10.005>
- Lyons, J. J., Dietterich, H. R., Patrick, M. P., & Fee, D. (2021). High-speed lava flow infrasound from Kilauea's fissure 8 and its utility in monitoring effusion rate. *Bulletin of Volcanology*, 83(11), 66. <https://doi.org/10.1007/s00445-021-01488-7>
- Marchese, F., Genzano, N., Neri, M., Falconieri, A., Mazzeo, G., & Pergola, N. (2019). A multi-channel algorithm for mapping volcanic thermal anomalies by means of Sentinel-2 MSI and Landsat-8 OLI data. *Remote Sensing*, 11(23), 2876. <https://doi.org/10.3390/rs11232876>
- Marchetti, E., Ripepe, M., Campus, P., Le Pichon, A., Vergoz, J., Lacanna, G., et al. (2019). Long range infrasound monitoring of Etna volcano. *Scientific Reports*, 9(1), 1–10. <https://doi.org/10.1038/s41598-019-54468-5>
- Marcillo, O., Arrowsmith, S., Blom, P., & Jones, K. (2015). On infrasound generated by wind farms and its propagation in low-altitude tropospheric waveguides. *Journal of Geophysical Research: Atmosphere*, 120(19), 9855–9868. <https://doi.org/10.1002/2014JD022821>
- Massimetti, F., Coppola, D., Laiolo, M., Valade, S., Cigolini, C., & Ripepe, M. (2020). Volcanic hot-spot detection using SENTINEL-2: A comparison with MODIS-MIROVA thermal data series. *Remote Sensing*, 12(5), 820. <https://doi.org/10.3390/rs12050820>
- Matoza, R. S., Fee, D., & Garcés, M. A. (2010). Infrasonic tremor wavefield of the Pu'u "O" crater complex and lava tube system, Hawaii, in April 2007. *Journal of Geophysical Research*, 115(12), 1–16. <https://doi.org/10.1029/2009JB007192>
- McComas, S., Arrowsmith, S., Hayward, C., Stump, B., & McKenna Taylor, M. H. (2022). Quantifying low-frequency acoustic fields in urban environments. *Geophysical Journal International*, 229(2), 1152–1174. <https://doi.org/10.1093/gji/ggab525>
- Michellier, C., Syavulisembo, A. M., Lagmouch, M., & Kervyn, F. (2016). *Limites administratives - Ville de Goma - Province du Nord-Kivu (République Démocratique du Congo) (Series 'Pr)*. Musée Royal de l'Afrique Centrale.

- Moore, C., Wright, T., Hooper, A., & Biggs, J. (2019). The 2017 eruption of Erta 'Ale volcano, Ethiopia: Insights into the shallow axial plumbing system of an incipient mid-ocean ridge. *Geochemistry, Geophysics, Geosystems*, 20(12), 5727–5743. <https://doi.org/10.1029/2019GC008692>
- Murphy, S. W., de Souza Filho, C. R., Wright, R., Sabatino, G., & Correa Pabon, R. (2016). HOTMAP: Global hot target detection at moderate spatial resolution. *Remote Sensing of Environment*, 177, 78–88. <https://doi.org/10.1016/j.rse.2016.02.027>
- Oth, A., Barrière, J., D'Oreye, N., Mavonga, G., Subira, J., Mashagiro, N., et al. (2017). KivuSNet: The first dense broadband seismic network for the Kivu rift region (Western Branch of East African rift). *Seismological Research Letters*, 88(1), 49–60. <https://doi.org/10.1785/0220160147>
- Patrick, M. R., Orr, T., Sutton, A. J., Lev, E., Thelen, W., & Fee, D. (2016). Shallowly driven fluctuations in lava lake outgassing (gas pistonning), Kilauea Volcano. *Earth and Planetary Science Letters*, 433(November), 326–338. <https://doi.org/10.1016/j.epsl.2015.10.052>
- Richardson, J. P., Waite, G. P., & Palma, J. L. (2014). Varying seismic-acoustic properties of the fluctuating lava lake at Villarrica volcano, Chile. *Journal of Geophysical Research: Solid Earth*, 119(7), 5560–5573. <https://doi.org/10.1002/2014JB011002>
- Ripepe, M., Marchetti, E., Bonadonna, C., Harris, A. J. L., Pioli, L., & Ulivieri, G. (2010). Monochromatic infrasonic tremor driven by persistent degassing and convection at Villarrica Volcano, Chile. *Geophysical Research Letters*, 37(15), 2–7. <https://doi.org/10.1029/2010GL043516>
- Rosenblatt, B. B., Johnson, J. B., Anderson, J. F., Kim, K., & Gauvain, S. J. (2022). Controls on the frequency content of near-source infrasound at open-vent volcanoes: A case study from Volcán Villarrica, Chile. *Bulletin of Volcanology*, 84(12), 1–17. <https://doi.org/10.1007/s00445-022-01607-y>
- Smink, M. M. E., Assink, J. D., Bosveld, F. C., Smets, P. S. M., & Evers, L. G. (2019). A three-dimensional array for the study of infrasound propagation through the atmospheric boundary layer. *Journal of Geophysical Research: Atmospheres*, 124(16), 9299–9313. <https://doi.org/10.1029/2019JD030386>
- Smittarello, D., Grandin, R., Jaspard, M., Derauw, D., Oreye, F., Shreve, T., et al. (2023). Nyiragongo crater collapses measured by multi-sensor SAR amplitude time series. *Authorea*, 26. <https://doi.org/10.22541/essoar.167979224.40405342/v1>
- Smittarello, D., Smets, B., Barrière, J., Michellier, C., Oth, A., Shreve, T., et al. (2022). Precursor-free eruption triggered by edifice rupture at Nyiragongo volcano. *Nature*, 609(7925), 83–88. <https://doi.org/10.1038/s41586-022-05047-8>
- Syavuliseambo, A. M., Kervyn, F., Lennert, M., Wolff, E., & Michellier, C. (2021). Spatio-temporal location of population: Strengthening the capacities of sudden hazards risk management in Goma, DRC. *International Journal of Disaster Risk Reduction*, 66, 102565. <https://doi.org/10.1016/j.ijdrr.2021.102565>
- Thelen, W., Waite, G., Lyons, J., & Fee, D. (2022). Infrasound observations and constraints on the 2018 eruption of Kilauea Volcano, Hawaii. *Bulletin of Volcanology*, 84(8), 1–24. <https://doi.org/10.1007/s00445-022-01583-3>
- Theys, N., Brenot, H., Smedt, I. D., Lerot, C., Hedelt, P., Loyola, D., et al. (2021). Global monitoring of volcanic SO<sub>2</sub> degassing using Sentinel-5 precursor Tropomi. In *2021 IEEE International geoscience and remote sensing symposium IGARSS* (pp. 1911–1914). <https://doi.org/10.1109/IGARSS47720.2021.9554664>
- Theys, N., De Smedt, I., Yu, H., Danckaert, T., Van Gent, J., Hörmann, C., et al. (2017). Sulfur dioxide retrievals from TROPOMI onboard Sentinel-5 Precursor: Algorithm theoretical basis. *Atmospheric Measurement Techniques*, 10(1), 119–153. <https://doi.org/10.5194/amt-10-119-2017>
- Theys, N., Hedelt, P., De Smedt, I., Lerot, C., Yu, H., Vlietinck, J., et al. (2019). Global monitoring of volcanic SO<sub>2</sub> degassing with unprecedented resolution from TROPOMI onboard Sentinel-5 Precursor. *Scientific Reports*, 9(1), 2643. <https://doi.org/10.1038/s41598-019-39279-y>
- Ulivieri, G., Ripepe, M., & Marchetti, E. (2013). Infrasound reveals transition to oscillatory discharge regime during lava fountaining: Implication for early warning. *Geophysical Research Letters*, 40(12), 3008–3013. <https://doi.org/10.1002/grl.50592>
- Valade, S., Ripepe, M., Giuffrida, G., Karume, K., & Tedesco, D. (2018). Dynamics of Mount Nyiragongo lava lake inferred from thermal imaging and infrasound array. *Earth and Planetary Science Letters*, 500, 192–204. <https://doi.org/10.1016/j.epsl.2018.08.004>
- Walwer, D., Wauthier, C., Barrière, J., Smittarello, D., Smets, B., & d'Oreye, N. (2023). Modeling the intermittent lava lake drops occurring between 2015 and 2021 at Nyiragongo volcano. *Geophysical Research Letters*, 50(8), e2022GL102365. <https://doi.org/10.1029/2022GL102365>
- Watson, L. M., Dunham, E. M., & Johnson, J. B. (2019). Simulation and inversion of harmonic infrasound from open-vent volcanoes using an efficient quasi-1D crater model. *Journal of Volcanology and Geothermal Research*, 380, 64–79. <https://doi.org/10.1016/j.jvolgeores.2019.05.007>
- Wright, R., Blackett, M., & Hill-Butler, C. (2015). Some observations regarding the thermal flux from Earth's erupting volcanoes for the period of 2000 to 2014. *Geophysical Research Letters*, 42(2), 282–289. <https://doi.org/10.1002/2014GL061997>
- Yamakawa, K., Ichihara, M., Ishii, K., Aoyama, H., Nishimura, T., & Ripepe, M. (2018). Azimuth estimations from a small aperture infrasonic array: Test observations at Stromboli volcano, Italy. *Geophysical Research Letters*, 45(17), 8931–8938. <https://doi.org/10.1029/2018GL078851>
- Yang, Y., & Ritzwoller, M. H. (2008). Characteristics of ambient seismic noise as a source for surface wave tomography. *Geochemistry, Geophysics, Geosystems*, 9(2), Q02008. <https://doi.org/10.1029/2007GC001814>

## References From the Supporting Information

- McNamara, D. E., & Buland, R. P. (2004). Ambient noise levels in the continental United-States. *Bulletin of the Seismological Society of America*, 94(4), 1517–1527. <https://doi.org/10.1785/012003001>